A98-31701

ICAS-98-7,4,3

A NEW PROCEDURE FOR SIMULATING ROTOR/STATOR INTERACTION IN TURBOMACHINERY

Wu, Xian Hong and Chen, Mao Zhang
Division 404, Jet Propulsion Dept.
Beijing University of Aeronautics & Astronautics
Beijing, 100083. P.R.China

ABSTRACT

A new numerical method is presented in this paper to simulate rotor / stator interaction in turbomachinery by use of a disturbance vortex method. By conducting a decomposition operation over flow quantities, the Lagrangian vortex method is used to capture the convective process of the disturbance vortex, and the deterministic vortex scheme to approximate the viscous diffusion process. The application of Baldwin-Lomax turbulence model in wakes is developed, so as to overcome the difficulty in continuously tracing moving wake centerlines encountered by other numerical methods and the difficulties such as the much higher calculated viscosity in the outer region than that in the boundary regions. The agreement between the computational and experimental results is generally good, which shows that the present method is reliable. The result also shows that this method can be used as a new tool for analyzing unsteady flow and mixing phenomena in turbomachinery.

Key Words: Turbomachinery, Rotor-Stator Interaction, Disturbance Vortex Method.

1. INTRODUCTION

It is well recognized that turbomachinery flow fields are inherently unsteady, this unsteadiness includes many factors. There are three dominant causes of unsteadiness related rotor and stator interaction. The first is wake / downstream blade interaction. The second is upstream blade / downstream blades potential interaction. The third is upstream vortex / downstream blade interaction. For modern transonic turbomachines, as pointed by Jung et al.(1996), if the velocity is sufficiently high at the interface between rotor and stator, then the effects of upstream unsteadiness on the downstream is much stronger than that of the downstream on the upstream.

The disturbance vortex method presented in this paper has many advantages in simulating unsteady flow in turbomachinery. These include: (1)it is convenient for the vortex method to cope with the complex boundaries in unsteady flow, such as the complicated transformation of meshes encountered in the finite-differential method. (2)using a Lagrangian frame, the unsteady mechanism can be described directly and conveniently by the process of upstream wakes and other vortices moving downstream. In addition, it also has obvious advantage in applying Baldwin-Lomax turbulence model in wakes by using this method. As early as 1970s, Leonard(1979) proposed this method in studying the development of three-dimensional turbulence spot. Although the equations and the described phenomenon of Leonard are different from those in this paper, the basic ideas are the same. In view of its inherent advantages, the application in simulating unsteady flow in turbomachinery is developed.

2. NUMERICAL METHOD

2.1 Governing equations

The vorticity dynamic equation for two dimensional, viscous compressible flow is:

$$\frac{\partial \omega}{\partial t} + (V \cdot \nabla)\omega = -\omega(\nabla \cdot V) + \nu \nabla^2 \omega \qquad (1)$$

Substituting ω and V of Eq.(1) by $\omega = \overline{\Omega} + \omega'$, $V = \overline{U} + u'$, respectively, one obtains:

$$\frac{\partial \overline{\Omega}}{\partial t} + \frac{\partial \omega'}{\partial t} + (\overline{U} \cdot \nabla)\overline{\Omega} + (\overline{U} \cdot \nabla)\omega' + (u' \cdot \nabla)\overline{\Omega} + (u' \cdot \nabla)\omega' = -\overline{\Omega}(\nabla \cdot \overline{U}) - \omega'(\nabla \cdot \overline{U}) - \overline{\Omega}(\nabla \cdot u') - \omega'(\nabla \cdot u') + \nu \nabla^2 \overline{\Omega} + \nu \nabla^2 \omega' \qquad (2)$$

where $\overline{\Omega} = \nabla \times \overline{U}$ is time-averaged vorticity, and $\omega' = \nabla \times u'$ disturbance vorticity.

If the Mach number of time-averaged velocity is not very high, we can assume that the volume expansion corresponding to disturbance velocities be zero:

$$\nabla \cdot u' = 0 \qquad (3)$$

When the Mach number increases and the circumferential non-uniformity increases, the error resulting from this assumption will increase. However, the benefit of employing this assumption in saving computer time is obvious. Further discussion about this assumption can be referred to [4].

Performing time-averaging operation to Eq. (2), and

applying $\int_0^T q'\,dt = 0$, $(q = \omega, V)$, $\frac{\partial \overline{\Omega}}{\partial t} = 0$, we obtain the final equation for disturbance vorticity:

$$\frac{d\omega'}{dt} = -(u'\cdot\nabla)\overline{\Omega} - \omega'(\nabla\cdot\overline{U}) + \overline{(u'\cdot\nabla)\omega'} + \nu\nabla^2\omega' \quad (4)$$

where d/dt stands for material derivative. In the case of laminar flow, the viscosity is, $\nu = \nu_l$, for turbulent flow $\nu = (\nu_l + \nu_t)$, ν_l, ν_t the laminar and turbulent viscosity, respectively. In this paper, ν_t was predicted by Baldwin-Lomax (1978) turbulence model.

2.2 Initial and boundary conditions

The initial condition can be specified as follows. We take a single-stage compressor as an example to describe the method (Fig.1). If the relative steady solutions of rotor and stator are known, which can be written as $\overline{Q}_r(\bar{x}, V_r t)$ and $\overline{Q}_s(\bar{x})$, then the initial condition can be written as:

$$q'(x,y,t_0) = \begin{cases} \overline{Q}_r(x,y) - \overline{Q}_{(axi)}(x) & \bar{x} = \bar{x}_1 \\ 0 & \bar{x} \neq \bar{x}_1 \end{cases} \quad (5)$$

where $\overline{Q}_{(axi)}$ is the circumferential averaged value of $\overline{Q}_r$, and where $\bar{x}(x,y)$ stands for the coordinate of a point in the flow field, V_r is the circumferential velocity of rotor.

On the solid wall, the no-penetration and no-slip conditions should be satisfied:

$$\vec{u}'.n = 0 \quad (6)$$

$$\vec{u}'.\tau = 0 \quad (7)$$

where n, τ are, respectively the normal and tangent unit vectors on the solid wall.

At upstream boundary, one can obtain the upstream boundary condition for disturbance variables at time t, according to the same idea as obtaining Eq. (5),:

$$q'(x,y,t) = \overline{Q}_r(x, y - Wt) - \overline{Q}_{(axi)}(x) \quad (8)$$

where $t = t_0 + k\Delta t$, $(1 \le k \le M)$, $\Delta t = T/M$, time period, $T = P_r/V_r$, P_r is rotor blade spacing, and M is the number of time steps in one period T. So the upstream boundary condition at any time step can be given as above.

On geometric boundaries in a single passage, if the rotor and stator have the same numbers of blades, the simple periodic condition holds:

$$q(x,y,t) = q(x, y + P_s, t) \quad (9)$$

where P_s is the stator blade spacing. and (x, y) streamwise and transverse coordination. If the rotor spacing differs from that of stator (Fig.1), one has to use the 'phase-shift periodic boundary condition':

$$q(x,y,t) = q(x, y + P_s, t + \Delta T) \quad (10)$$

where $\Delta T = (P_r - P_s)/W$。

As this boundary condition is rather complicated when the vortex method is used, we will not discuss it here in detail. The reader who concerns this can refer to Wu[1].

2.3 Turbulence model

Baldwin and Lomax turbulence model faces two difficulties when it is used to calculate unsteady rotor / stator interaction: one is the much higher computed viscosity in the outer region than that in the boundary regions according to the original notations of y_{MAX} and F_{MAX} in Baldwin and Lomax model, which resulted from that the positions of wakes is far from the boundary; the other is the difficulty in continuously tracing moving wake centerlines so as to obtain the perpendicular distance of y to wake centerlines in calculating the factor of Klebanoff, $F_{KLEB(y)}$.

Fig. 1 A typical configuration of a single-stage compressor

The reason for the first problem is that there is a high vorticity region in the wakes so that $F(y)$ obtains its maximum value in the outer layer of the boundary. To overcome this problem, we redefine y as the smallest distance at which $F(y)$ meets the condition:

$$\frac{dF}{dy} = 0 \quad (11)$$

For the second problem, it is often encountered by finite-differential and finite-volume numerical methods. In this paper, as the vortex method is a Lagrangian frame, which has the advantage to trace the trajectories of wakes. For example, the positions of the wakes coming form upstream can be calculated and the centers of wake transported in the stator passage at different time in a period are located. All the center points in one period consist the centerline of wakes. It should be pointed out that in two-dimensional domain, the center point of the wake moving into the inlet of stator computational domain at any time be defined as the point where the direction of disturbance vorticity changes. The widths of wakes is defined as the center points, but the two boundaries of the wake is the point on the two side of the centerline where the gradient of the disturbance velocities changes most distinctly. Based on this definition, the widths of wakes can be defined at the inlet wakes of the stator and the positions at any time can be determined. See fig. 2

In the outer layer of the boundary, the total viscosity should include the combined effects of boundary and wake, so it is calculated as follows:

$$\mu_{tot} = \mu_t + \mu_w \tag{12}$$

where μ_t is the turbulence viscosity coefficient of boundary layers, μ_w the eddy viscosity of wakes. In the inner layer of the boundary, the effect of wakes is relatively weak, so the wake viscosity is negligible.

2.4 Computation procedure

In two-dimensional domain, the disturbance vorticity field can be represented by a set of discrete vortex particles[5]:

$$\omega'(r,t) = \sum_{j=1}^{N} \Gamma_j' f_\sigma(r - x_j(t)) \tag{13}$$

where N is the number of vortex particles, Γ_j' the circulation of j th vortex at time t, $f_\sigma = \frac{1}{\sigma^2} f(\frac{r}{\sigma})$, where σ is the radius of vortex particle, $f(r)$ shape function, in the present study, a Gauss core of second order is adopted, i.e. $f(r) = \frac{1}{\pi} e^{-r^2}$. r vector radius, $x_j(t)$ the location and respectively,

Applying the viscous splitting algorithm, the displacement and circulation variation of disturbance vortex caused by convective process are:

$$\vec{x}_2 = \vec{x}_1 + (\vec{\bar{U}} + \vec{u}')\Delta t \tag{14}$$

$$\Gamma_j'(t+\Delta t) = \Gamma_j'(t) + F[-u_j' \cdot \nabla \bar{\Gamma}_j - \Gamma_j'(\nabla \cdot \bar{U}_j) + \overline{(u_j' \cdot \nabla)\Gamma_j'}] \cdot \Delta t \tag{15}$$

where $F[]$ stands for integration scheme, $\bar{\Gamma}$ time-averaged circulation, S_j a vortex element area. The correlation $\overline{(u' \cdot \nabla)\Gamma'}$ can be obtained through summing up $u' \cdot \nabla \Gamma'$ of each time step and then performing time-averaging operation.

The contribution of viscous term on disturbance vorticity can be obtained by use of the deterministic vortex method. Here the method proposed by Fishelov (1990) was used, and the operator on vorticity can be written in the discrete form according to (13):

$$\nabla^2 \omega' = \sum_{j=1}^{N} [\Delta f_\delta(\vec{x}_i - \vec{x}_j)] \Gamma'_j(t) \tag{16}$$

where $\Delta = \nabla^2$. This is our work form for viscous term. $\vec{u}'(\vec{x}_1)$

The disturbance velocity includes the induced disturbance velocity, the expansion disturbance velocity and the potential velocity.

The disturbance velocity field induced by the vortex particles are evaluated as follows:

$$\vec{u}_v'(r,t) = \sum_{j=1}^{N} \Gamma_j' K_\delta(r - x_j(t)) \tag{17}$$

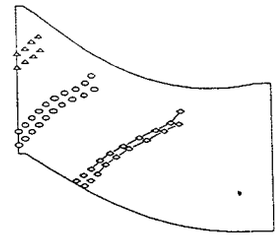

Fig. 2 The centerlines and half-width lines of wakes

where $K_\delta = K * f_\delta$, $K(r) = -\frac{(-y,x)}{2\pi|r|^2}$, and $*$ stands for convolution operator.

According to Bachleor (1967), the disturbance velocity associated with expansion rate H_m' is:

$$\vec{u}_e'(\vec{x},t) = \frac{1}{2\pi} \int H'_m \frac{\vec{r}}{r^3} dS'(\vec{x}) \tag{18}$$

where dS' stands for area. According to Eq.(3), the expansion rate of disturbance velocity $\nabla \cdot \vec{u}' = H'_m = 0$, so $\vec{u}_e' = 0$.

The disturbance velocity field consisted of $\vec{u}_e' + \vec{u}'_v$ usually can not meet boundary condition, so a potential disturbance velocity is added to ensure a no-penetrable condition on solid walls, i.e.

$$(\vec{u}_e' + \vec{u}'_v) \cdot n = -\vec{u}'_p \cdot n \tag{19}$$

The potential disturbance velocity is the gradient of a potential function, and the potential function is the solution of Laplace equation:

$$\nabla^2 \phi = \frac{\partial^2 \phi}{\partial x^2} + \frac{\partial^2 \phi}{\partial y^2} = 0 \tag{20}$$

under the boundary condition of Eq.(19) on solid walls and unsteady boundary condition on geometric boundaries of Eq. (10):

$$\nabla \phi(x) = \vec{u}'_p \tag{21}$$

The no-slip condition on solid walls can be calculated as [5]. i .e. the strength of the vortex sheet must meet the condition :

$$\Gamma' = \vec{u}' \cdot \tau \tag{22}$$

where $\vec{u}'$ stands for the sliding velocity on solid walls. τ a unit vector tangent to the solid wall. At any time step, the motion of vortex sheet in the boundary is determined as [5], once they enter into main flow region, they are converted into vortex particles, while keeping their vorticity strength unchanged. If they go into the boundary layer, their effects can be negligible.

3. VALIDATION OF THE METHOD

To check the present method, we calculated the unsteady

flows at 50 span in the first stage of NASA-67 compressor. As the experimental data are relatively rare, here the calculated results--unsteady velocity correlations $\overline{u'v'}$, $\overline{u'^2}$, $\overline{v'^2}$ --are compared with experimental data (Hathaway (1986)) at four axial positions: 0, 20, 50 and 100 percent of chord, see Fig.3, Fig. 4 and Fig. 5. These contours show that the prediction and experimental data in [3] are in general agreement, especially $\overline{u'v'}$ and $\overline{v'^2}$. Although $\overline{u'^2}$ is not very good near the stator leading edge, satisfactory agreement between the computational and experimental results at 20, 50 and 100 percent of chord is obtained. From the prediction we can conclude that the present method is reliable.

4. RESULTS AND DISCUSSIONS

Based on the method. we calculate the unsteady flows due to rotor/stator interaction in a high loading transonic compressor stage. The main features of the stage are listed on Table 1. The flow field on the stream surface at middle span was simulated. An H-type grids employed with the node number (47+43)*33, and 47, 43, represent axial grids of rotor and stator, respectively; 33, circumferential grid. The Reynolds number is 0.904×10^7 based on the stator chord length and stator inlet velocity. One time period is divided into twenty time steps.

(1) Cutting of Wakes

Fig. 6 shows the disturbance vorticity contours at different time instants in a period after convergent status is obtained. We see from the figures that when a wake is sweeping the stator blades, a complete wake is cut into several separate segments. Along with the vortex particles move into the stator passage, there appears a tendency that the particles are pushed towards the pressure surface of stator blades. In additional, there seem to be two processes during the particles moving downstream, i.e. (1) decentralization-centralization, Fig. 6a-f, with two vorticity concentration areas formed (see A and B) at circle 4.5, the strengths of which are -2.6 and -1.1, respectively; (2) centralization-decentralization, Fig. 6g--j, with vorticity concentration areas decentralized and broken near the exit of stator blades, where the pressure tends towards uniform distribution. The latter process indicates that as an interaction between wakes, vortices and boundary layers, a strong mixing process occurs, resulting in a mixing of main flow with fluid carrying highly concentrated vorticity. This coincides with the observation of Kerrebrock and Mikolajczak (1970).

Table.1 Airfoil Mean section Characteristics of a Single-Stage Compressor

	Rotor	Stator
stage pressure ratio	1.66	
U_{tip} (m/s)	441.	0
blade number	23	40
chord length (m)	0.1432	0.08115
solidity	1.491	1.442
radius ratio	0.41	0.51
aspect ratio	1.8	2.4
inlet angle (deg)	43.24	47.28
outlet angle (deg)	41.63	0.

(2) Influence of Unsteadiness on Incidence

To study the influence of the rotor-stator interaction on incidence. Fig. 7 shows the variation of disturbance incidence (exclusive of averaged incidence) with time in a period, where the time axis also represents the number of circle. The result indicates that the unsteadiness has a large influence on incidence. The maximum is as high as 2.84 degrees, while the minimum is -0.374 degrees. It also shows that the distribution is similar to a sine shape, but the above and the lower are not symmetry. The positions of the maximum and the minimum is related to the relative positions of rotor and stator. As the ratio of rotor and stator is 1.74, the disturbance incidence increases if the wakes sweep the stator and vice verse, with the direction of incidence will change. From above, it can be concluded that the load of a compressor will change in a period with the upstream unsteadiness, and this unsteadiness has a great effect on incidence.

(3) Amplitudes of Disturbance Velocities

To study the decaying characteristic of unsteadiness, the amplitudes of the first harmonic of unsteady streamwise and transverse velocities at four axial location are shown in Fig.8 and Fig.9. (The reference velocity is the steady velocity at the stator leading edge). $x/c = -.015$ stands for a location of 1.5 percent axial chord upstream of stator: $x/c = 0.168$ and $x/c = 0.75$, two axial positions between the leading and the trailing edges: $x/c = 1.018$ represents a location of 1.8 percent axial chord downstream. From these figures, we can see that the streamwise and the transverse disturbance velocities near the solid walls are higher than those above the boundary at $x/c = -.015$. while the disturbance velocities are smaller in the main flow. There are two large fluctuations of streamwise disturbance at $x/c = 0.168$ and $x/c = 0.75$, occurring at about 10 percent pitch near the pressure surface, with magnitude as high as 18% and 14% of V_0. Also, the maximum amplitude of the transverse disturbance velocity has a large point at 30 percent pitch near the pressure surface and the axial position $x/c = 0.168$. This is different from the turbulence

fluctuation, which is much stronger in boundary layer near solid surfaces. And at the position $x / c = 1.018$, the amplitude of streamwise disturbance velocity is smallest of the four axial positions, where the disturbance velocity tends towards uniform distribution. The transverse disturbance velocity has the same characteristic as the streamwise one. But a large amplitude of the transverse velocity fluctuation is near pressure surface. From Fig. 8 and Fig.9, we can see that the maximum amplitude of disturbance velocity occurs near the axial position $x / c = 0.168$. This is the result of the chopping of rotor wakes by the stator leading edge. Along the stator chord, the streamwise velocity decreases gradually.

(4) Amplitudes of Disturbance Pressure

The amplitude of the first harmonic of the unsteady pressure on the stator blade surface is shown in Fig. 10 and Fig. 11. The amplitude is normalized by the inlet steady total pressure. For this configuration, the unsteady pressure on the pressure surface obtains the maximum near the leading edge, and it decays along the stator chord. This effect is much more significant from leading edge to 10 percent of stator's axial chord. From this position to the trailing edge, the decaying trend becomes slower, and the minimum occurs at the trailing edge. On the suction surface, the amplitude decays gently and there is a little increase from 30 to 40 percent of the stator chord. After this position, the amplitude begins to decrease, and it is near zero at the trailing edge . These decaying trends of unsteady pressure on solid walls agree with Ho and Lakshimnarayana (1996), who observed the decay of unsteady pressure.

5. CONCLUDING REMARKS

The unsteady flow caused by rotor-stator interaction in turbomachinery is simulated by employing a Lagrangian-disturbance vortex method proposed in the present paper. the algorithm describes the unsteady process by tracing the trajectories of vortices directly and recording the changes of the disturbance vorticity. The Baldwin-Lomax turbulence model is applied in boundary layer and wakes to overcome the difficulty encountered by other numerical methods, such as the difficulty in continuously tracing moving wake centerlines and the much higher computed viscosity in the outer region than that in the boundary layers. It is concluded that the disturbance vortex method presented can be used as a new tool for analyzing unsteady flow in turbomachinery.

REFERENCES

Jung, A.R, Mayer, J.F, and Stetter, H "Simulation of 3D-Unsteady Stator/Rotor Interaction in Turbomachinery Stages of Arbitrary Pitch Ratio " ASME Paper 96-GT-69, 1996.

Baldwin, B.S., Lomax, H., 1978, "Thin Layer Approx. and Algebraic Model for Separated Turbulent Flows", AIAA 78-257.

Leonard, A., "Vortex Simulation of Three-Dimensional Spotlike Disturbance in a Laminar Boundary Layer", 2nd Symposium on Turbance Shear Flows: July 2. Imperial College, 1979, 67-77.

Wu, X. H. "Vortex Simulation of Rotor/Stator Interaction in Turbomachinery" Ph.D. Dissteration, Beijing University of Aeronautics and Astronautics, (in Chinese) 1997 .

Chorin,A.J., "Numerical Study of slightly viscous flow" J. Fluid Mech., vol.57, 1973, 785-796

Fishelov, D, "A new vortex scheme for viscous flows". J. Comp. Phys., Vol , 86 , 1990 , 211-224.

Bachleor,G.K, "An Introduction of Fluid Dynamics" Combridge University Press. 1967.

M.D.,Hathaway, "Unsteady Flows in a Single-Stage Transonic Axial-Flow Fan Stator Row "
NASA-TM-88929, 1986

Kerrebrock. J.L, and Mikolajczak. A.A, "Intra-stator Transport of Rotor Wakes and Its Effect on Compressor Performance." ASME Paper 70-GT-39, 1970.

Y.-H, Ho, and Lakshminarayana, B., "Computation of Three-Dimensional Steady and Unsteady Flow Through a Compressor Stage " ASME Paper, GT-96-70, 1996.

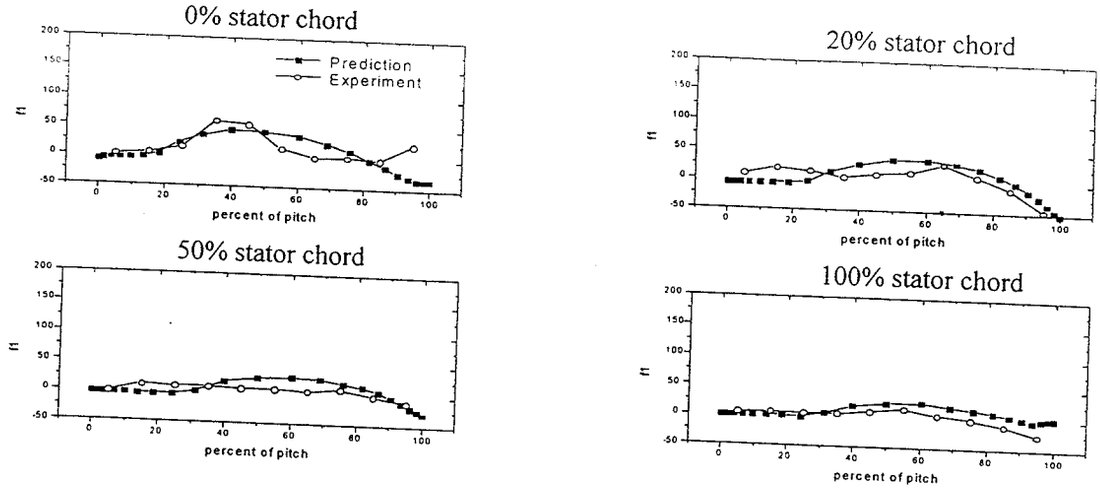

Fig. 3 Circumferential distribution of $\overline{u'v'}$ (m^2/s^2) for *NASA*-67 compressor

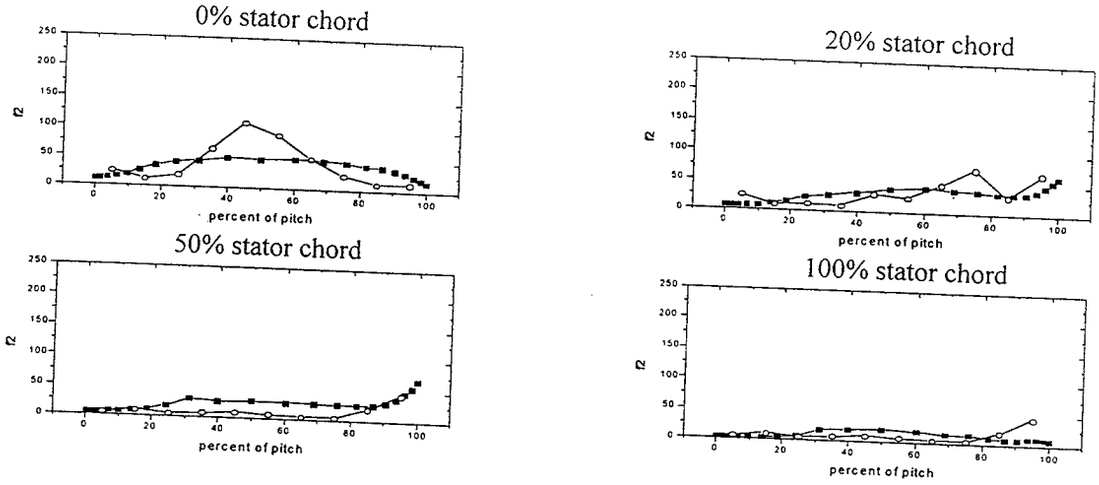

Fig. 4 Circumferential distribution of $\overline{u'^2}$ (m^2/s^2) for *NASA*-67 compressor

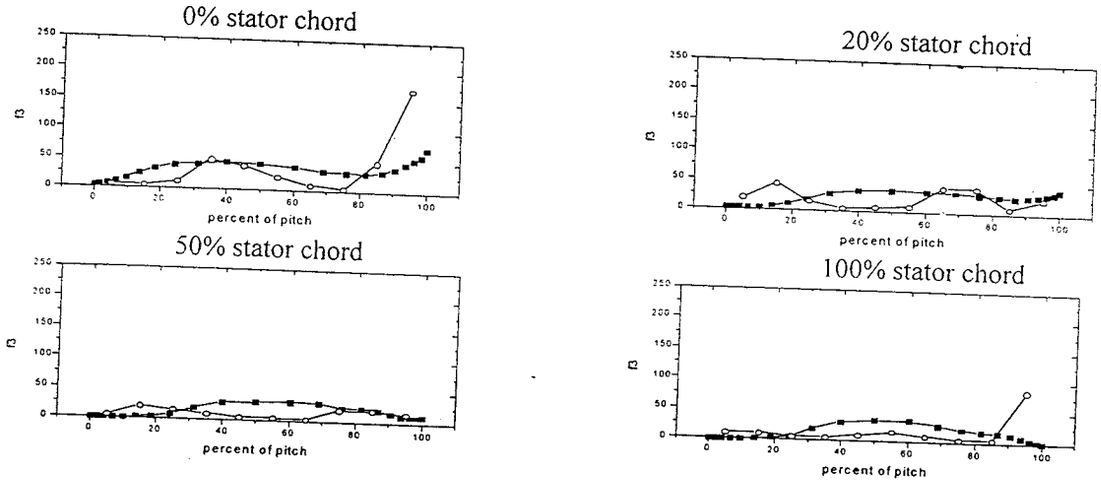

Fig. 5 Circumferential distribution of $\overline{v'^2}$ (m^2/s^2) for *NASA*-67 compressor

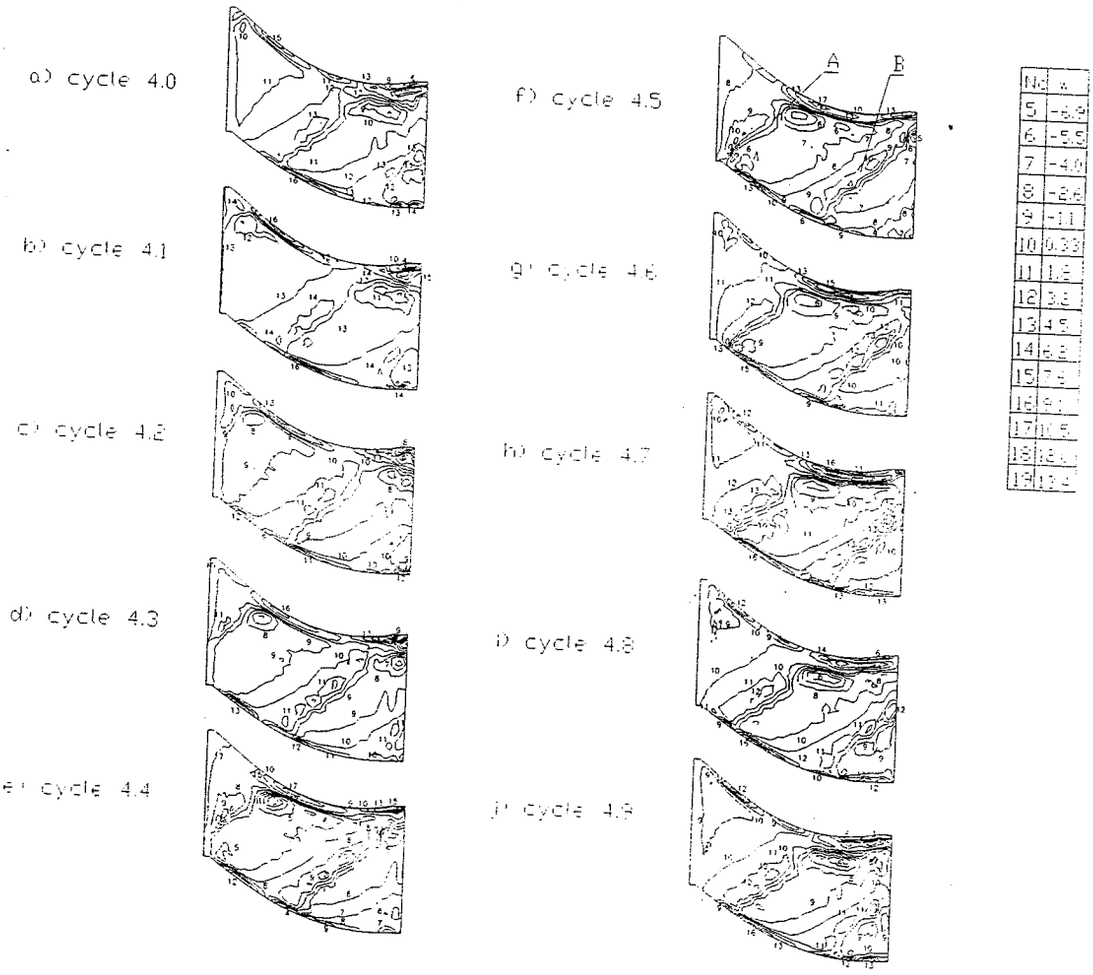

Fig. 6 Disturbance vorticity contours at different instants in one period

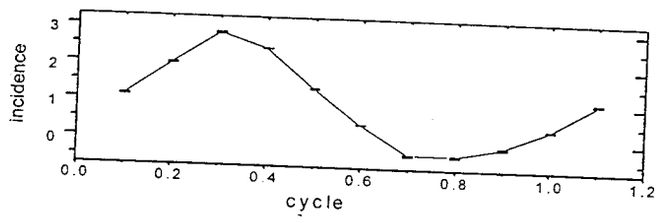

Fig. 7 Variation of disturbance incidence with time in one period

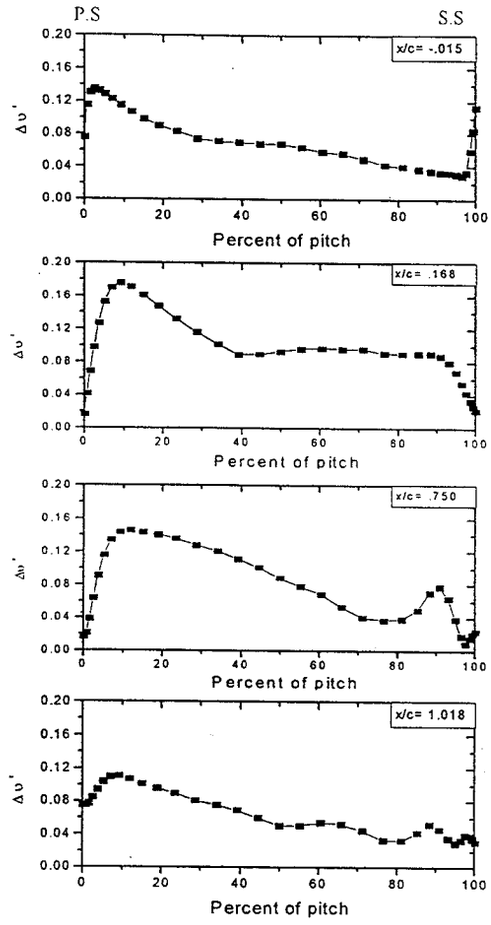

Fig. 8 First harmonic amplitude of the streamwise disturbance velocities

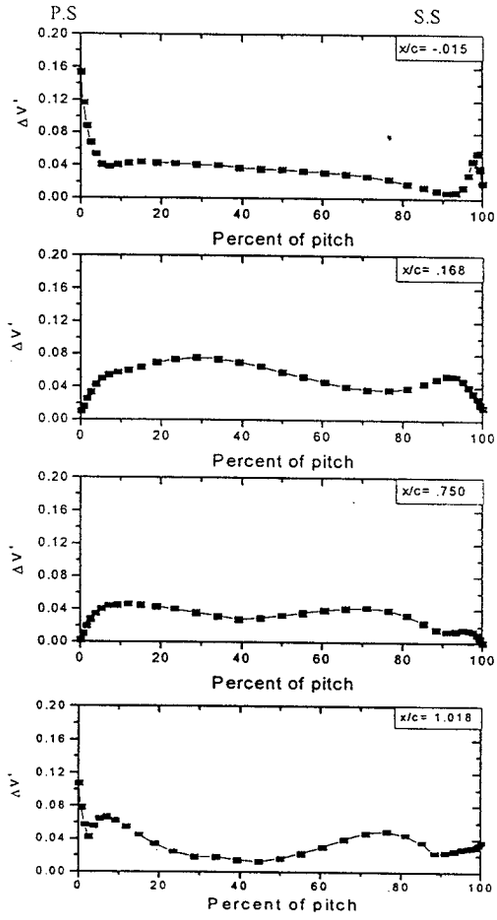

Fig. 9 First harmonic amplitude of the transverse disturbance velocities

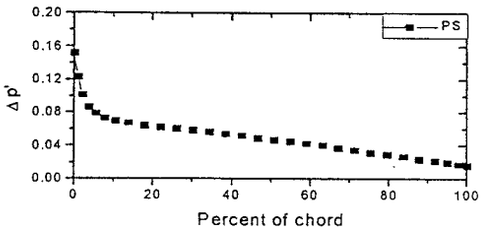

Fig.10 First harmonic amplitude of unsteady pressure on pressure surface

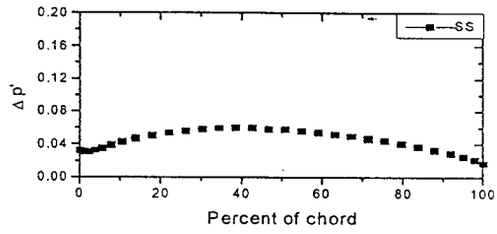

Fig.11 First harmonic amplitude of unsteady pressure on suction surface